Electrochimica Acta 56 (2011) 5926–5933

Contents lists available at ScienceDirect

Electrochimica Acta

journal homepage: www.elsevier.com/locate/electacta

Performance of a multipurpose research electrochemical reactor

E.R. Henquín, J.M. Bisang*

Programa de Electroquímica Aplicada e Ingeniería Electroquímica (PRELINE), Facultad de Ingeniería Química, Universidad Nacional del Litoral, Santiago del Estero 2829, S3000AOM Santa Fe, Argentina

ARTICLE INFO

Article history:
Received 2 March 2011
Received in revised form 25 April 2011
Accepted 28 April 2011
Available online 6 May 2011

Keywords:
Bipolar electrodes
Current distribution
Electrochemical reactors
Electrosynthesis
Filter press
Multipurpose reactor

ABSTRACT

This paper reports on a multipurpose research electrochemical reactor with an innovative design feature, which is based on a filter press arrangement with inclined segmented electrodes and under a modular assembly. Under bipolar connection, the fraction of leakage current is lower than 4%, depending on the bipolar Wagner number, and the current distribution is closely uniform. When a turbulence promoter is used, the local mass-transfer coefficient shows a variation of ±10% with respect to its mean value. The fluidodynamics of the reactor responds to the dispersion model with a Peclet number higher than 10. It is concluded that this reactor is convenient for laboratory research.

1. Introduction

The development and optimization of electrochemical processes require experiments in reactors with a well-known fluidodynamics, uniform mass transfer conditions at the electrode surface and without any current distribution. Thus, the reactor can be represented by an ideal mathematical model. Likewise, it is necessary that the reactor should present a modular construction allowing the use of different turbulence promoters as well as separators between the electrodes. It may be electrically connected in either a monopolar or bipolar arrangement. A reactor fulfilling these conditions becomes of interest for laboratory research because it represents a multipurpose unit.

The filter press configuration is a useful geometry to construct a research reactor. Thus, Walsh [1] describes the FM01-LC laboratory reactor, as a simpler and scaled-down version of the FM21-SP reactor, which is used in the chlor-alkali industry. The FM01-LC electrolyser was extensively investigated. Thus, mass-transfer studies were reported in [2–5], the hydrodynamic behaviour was analysed in [6–9] and the current distribution in [10]. Similar studies have been informed for another commercial filter-press reactor, the ElectroSyncell® cell [11]. The hydrodynamic behaviour was reported in [12] and it was complemented with a study of flow visualization [13]. Likewise, the hydrodynamic and mass-transfer behaviour were characterized for a homemade electrochemical laboratory [14] or pilot-plant [15] filter-press reactor.

Hoechst-Uhde [16] developed a commercial bipolar filter-press reactor with louver-type plate electrodes, where the electrolysis gases formed at the front edge are fed to the rear of the electrodes and do not interfere with the Ohmic drop. Likewise, inclined electrodes are also interesting in electrochemical engineering to enhance the mass-transfer coefficient [17].

The aim of this paper is to study a filter press electrochemical reactor with inclined electrodes for its use as research equipment. Thus, mass-transfer characteristics, residence time distribution and the effect of the leakage current on the current distribution in the case of a bipolar connection are considered.

2. Experimental

Fig. 1 schematically shows a module of the flow-by electrochemical reactor formed by two Teflon plates with inclined segmented electrodes and one frame. Fig. 2(a) sketches a cross-section of a plate, which supports ten nickel electrodes, positioned near the separator and inclined 30° from the vertical to deviate the gases to the backside of the electrodes. This inclination angle is in the optimal range for gas evolving electrodes [18]. Thus, in case of gas evolution at the electrodes the gases are deviated from the inter-electrode gap and the interference with the electrolyte Ohmic drop is minimized. The explode view of the segments in Fig. 2(b) shows the electrolyte and gases flows inside the plate. The projected area of each segment on the separator was 1 cm × 5 cm and the

* Corresponding author.
E-mail address: jbisang@fiq.unl.edu.ar (J.M. Bisang).

0013-4686/$ – see front matter © 2011 Elsevier Ltd. All rights reserved.
doi:10.1016/j.electacta.2011.04.115

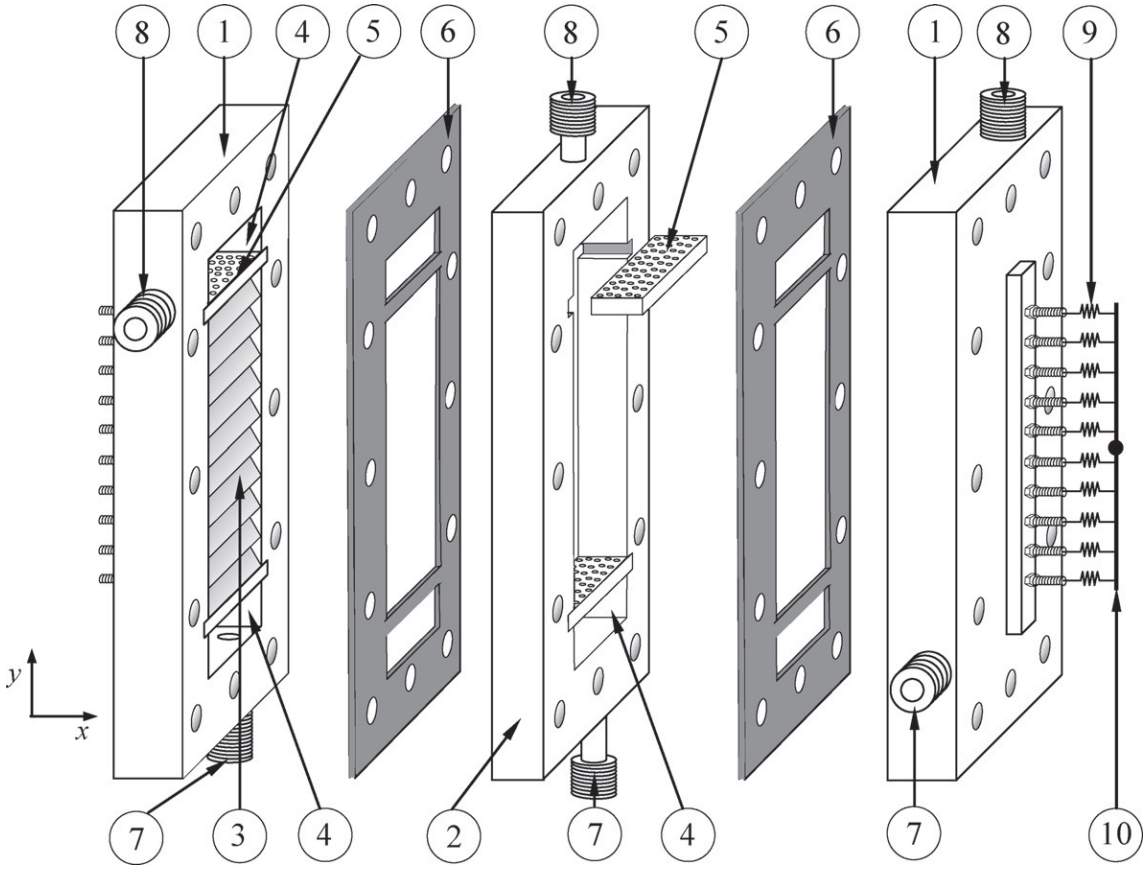

Fig. 1. Exploded view of one module of the electrochemical reactor. (1) plates; (2) frame; (3) segmented inclined electrodes; (4) electrolyte chambers; (5) flow distributor plates; (6) gaskets; (7) electrolyte inlets; (8) electrolyte outlets; (9) calibrated resistors; (10) electrical connection to the electrodes.

backside of each segment was covered with epoxy resin to make it non conductive. In the study of current distribution, some experiments were also performed with segments of stainless steel as cathode. The lower and upper parts of the plate present a chamber for the inlet and outlet of the electrolyte, and to achieve more uniform mass-transfer conditions along the reactor, flow distributor plates with 144 holes, 1.5 mm diameter, were arranged in the inlet and outlet of the electrolyte to the electrode region. Two plates were joined by tie rods to build up a cell, and the electrical connection in series of two cells formed an electrochemical reactor with one bipolar electrode. The modular assembly of this reactor admits either a separator or a frame between the plates with inclined electrodes. Preliminary experiments for current distribution performed with a reinforced cation exchange membrane between the plates showed a high scattering of the results because of the different positioning of the membrane along the electrode, because of the electrolyte and gases flows, which masked the current distribution produced by the leakage current. To avoid this problem the membrane was replaced by a frame containing electrolyte, 17 mm thick, whose resistance was similar to those of the membrane.

A calibrated resistor made from constantan (Cu55Ni45) wire, 100 mm long, 1.5 mm diameter and approximately 0.02 Ω resistance, was intercalated between the backside of each segment and the current feeder. By measuring the Ohmic drop in the corresponding resistor, it was possible to determine the axial current distribution at each electrode or the calculation of the local mass-transfer coefficient. The influence of these resistors on the cell voltage is negligible due to the small value of its resistance. The data acquisition was performed with an analogue multiplexer commanded by a computer.

Owing to the special construction of this reactor, the segments drain the same current but, under bipolar connection, the manifolds for the supply and withdrawal of the electrolyte and products can produce leakage currents and current distribution at the reactor.

The reactor was made part of a flow circuit system consisting of a pump, a flow meter, a reservoir and connections to maintain the temperature at the preset value, 30 °C. The experiments for the study of current distribution were done galvanostatically and the electrolyte solution was 1 mol dm^{-3} of NaOH or 3 mol dm^{-3} of NaOH, being hydrogen- and oxygen-evolution the cathodic and anodic reactions, respectively.

The experiments for the characterization of mass-transfer were carried out potentiostatically in a monopolar arrangement. A saturated calomel reference electrode connected to a Haber-Luggin capillary was used, positioned near the working electrode. The test reaction was the electrochemical reduction of ferricyanide from solutions with $[K_3Fe(CN)_6] \cong 1 \times 10^{-2}$ mol dm^{-3}, $[K_4Fe(CN)_6] \cong 1 \times 10^{-2}$ mol dm^{-3}, in 1 mol dm^{-3} of NaOH as supporting electrolyte, while the reverse reaction occurred at the anode. Experiments were performed with an empty reactor, and also the plates and the frame were completely filled with plastic beads 3 mm diameter, in order to increase the mass-transfer coefficient and to make it independent of the position inside the reactor. The experiments were performed at 30 °C and nitrogen was bubbled in the reservoir for 1 h prior to the experiment in order to remove the dissolved oxygen.

The residence time distribution was analysed for the plate with inclined electrodes, for the frame and for the reactor with a monopolar arrangement separately. Flow dispersion curves were obtained using the stimulus-response method. As a stimulus, an impulse function was simulated by manually injecting

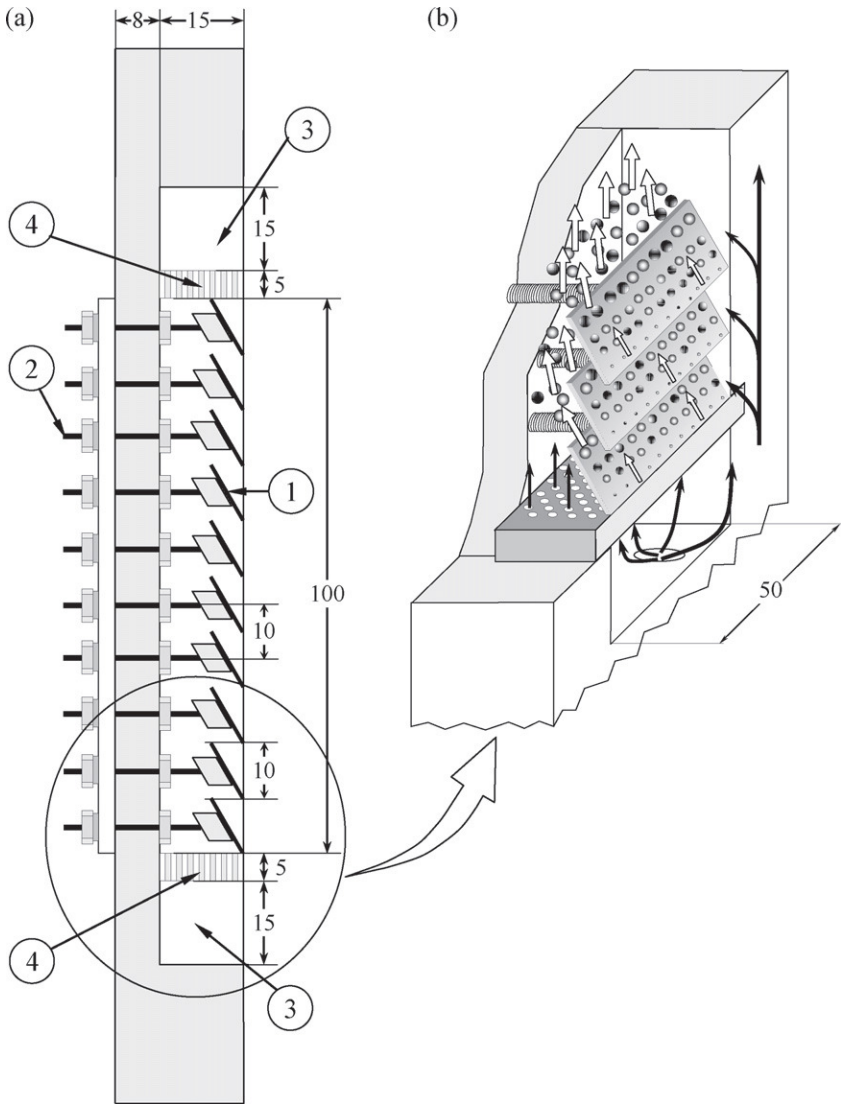

Fig. 2. (a) Cross-section of a plate with inclined electrodes. (1) segmented inclined electrodes; (2) electrical connection to the electrodes; (3) electrolyte chambers; (4) flow distributor plates. (b) Exploded view of the inclined segments showing the flows of electrolyte and gas. *Solid arrows*: electrolyte flow. *Hollow arrows*: gas flow. Dimensions in mm.

a 30 wt% NaOH solution, 0.2 cm^3, into the inlet for a short time. The electrolytic conductivity was monitored by means of a platinum conductivity cell, WTW model LTA 01, with a cell constant 0.114 cm^{-1} mounted on a T-piece in the reactor outlet. The conductimeter was connected to a digital multimeter to obtain conductance versus time. It was verified that a linear relation between conductivity and concentration takes place in the measure range.

3. Results and discussion

3.1. Current distribution studies

3.1.1. Mathematical modelling

In the following mathematical treatment the effect of the leakage current on the current distribution is analysed. Some simplifying assumptions are made:

(i) The metal phase of the electrodes is isopotential.
(ii) The current distribution in the direction of the electrode width is neglected.
(iii) The effect of the gases generated at the electrodes on the electrolyte resistivity is disregarded.
(iv) The electrodes are considered as parallel plates positioned in the middle point of the segments. The interelectrode gap used in the calculation was 27 mm, which takes into account the frame thickness, both gaskets and the mean value of the inclination of the segments. This assumption represents a fair approach because the inclination of the segments is small in comparison to the other dimensions.

The potential distribution was obtained by solving the Laplace equation in the solution phase including the electrolyte manifolds:

$$\frac{\partial^2 \phi_s(x,y)}{\partial x^2} + \frac{\partial^2 \phi_s(x,y)}{\partial y^2} = 0 \quad (1)$$

with the following boundary condition at the insulating walls

$$\left.\frac{\partial \phi_s(x,y)}{\partial x}\right|_{\text{insulating walls}} = \left.\frac{\partial \phi_s(x,y)}{\partial y}\right|_{\text{insulating walls}} = 0 \quad (2)$$

where ϕ_S (V) is the potential in the solution phase and x (m) and y (m) are the axial coordinates.

Table 1
Physicochemical properties and kinetic parameters used in modelling of current distribution.

Electrolyte resistivity, ρ_s, c_{NaOH} = 1 mol dm^{-3}	5.85×10^{-2} Ω m
Electrolyte resistivity, ρ_s, c_{NaOH} = 3 mol dm^{-3}	3.27×10^{-2} Ω m
Reversible cell potential	1.23 V
Tafel slope, b_a (nickel anode)	0.0435 V
Exchange current density, $j_{0,a}$ (nickel anode)	1×10^{-3} A m^{-2}
Tafel slope, b_c (nickel cathode)	0.0391 V
Exchange current density, $j_{0,c}$ (nickel cathode)	1×10^{-1} A m^{-2}
Tafel slope, b_c (stainless steel cathode)	0.0551 V
Exchange current density, $j_{0,c}$ (stainless steel cathode)	7.67×10^{-2} A m^{-2}

For secondary current distribution, the boundary conditions at the electrode surfaces are obtained by combining the Ohm's law, Eq. (3), with a kinetic expression.

$$j_{i,\,k}(y) = \left. -\frac{1}{\rho_s}\frac{\partial \phi_s(x,y)}{\partial x}\right|_{k\text{th electrode surface}} \quad (3)$$

where j (A m^{-2}) is the current density, i indicates the anodic or the cathodic reaction, k the electrode, i.e. terminal anode (A), bipolar electrode (B) or terminal cathode (C) and ρ_s (Ω m) is the electrolyte resistivity.

A Tafel equation was assumed for the kinetics at each electrode surface according to:

$$j(y) = j_0 \exp\left[\frac{\eta(y)}{b}\right] \quad (4)$$

being j_0 (A m^{-2}) the exchange current density, b (V) the Tafel slope and η (V) the overpotential, defined as

$$\eta(y) = \phi_m - \phi_0(y) - E_0 \quad (5)$$

where ϕ_m (V) is the potential in the metal phase, ϕ_0 (V) is the potential in the solution phase adjacent to the electrode surface and E_0 (V) is the reversible electrode potential.

The current, I (A), drained at each electrode surface was calculated as

$$I_k = W\int_0^L j_{i,k}\ dy \quad (6)$$

here L (m) is the electrode length and W (m) is the electrode width, and the leakage current, I^* (A), is given by

$$I^* = I_{A\text{ or }C} - I_B \quad (7)$$

The simultaneous and iterative solution of the above equations was performed by using the finite difference method with a home-made software utilizing the scientific computing platform Matlab. The calculation procedure was described in detail in [19]. Table 1 summarizes the kinetic and physicochemical parameters used in the modelling.

To quantify the predictive capability of the theoretical model, the mean relative deviation is introduced as

$$d_r = \frac{1}{N}\sum_{i=1}^{N}\frac{\left|j_{exp}(z_i) - j_{th}(z_i)\right|}{j_{th}(z_i)} \times 100 \quad (8)$$

where N is the number of experimental data and the subscripts "exp" and "th" denote the experimental and theoretical values, respectively. Lower values of d_r mean a close agreement between both distributions. All the parameters conditioning the secondary current distributions at the electrodes are lumped in the bipolar Wagner number, defined as [19]

$$Wa_{Bi} = \frac{b_a + b_c}{IR} \quad (9)$$

where R (Ω) is the by-pass resistance.

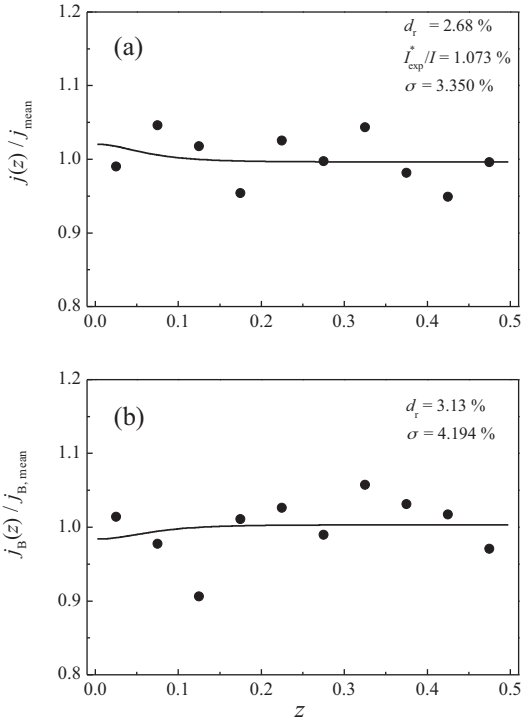

Fig. 3. Secondary current distribution for an electrochemical stack with one bipolar electrode. (a) terminal electrodes, (b) bipolar electrode. Anode: nickel. Cathode: nickel. c_{NaOH} = 3 mol dm^{-3}, R = 54.35 Ω, I = 4.999 A. Full line: theoretical prediction.

3.1.2. Experimental results of current distribution

Fig. 3 shows typical current distribution curves at the terminal and bipolar electrodes and the full lines correspond to the theoretical secondary current distribution obtained from the solution of the Laplace equation. For symmetry reasons, only one half of the stack was considered. The inlets of both cells were connected to a manifold and their outlets discharged directly to the reservoir via long hoses. Thus, the leakage current takes place only in the inlet manifold. A suitable prediction capability of the theoretical treatment, d_r near 3%, can be observed and the current distributions are uniform at both electrodes in spite of the slight scattering of the experimental results. Tables 2 and 3 summarize the results for different values of by-pass resistance of the manifolds, total current and cathode material. The mean relative deviation reported in columns 4 and 5 in Tables 2 and 3 reveals that the agreement between experimental and theoretical results is better for the terminal electrodes than for the bipolar one. This can be attributed to the higher scattering of the experimental results for the bipolar electrode. However, a reasonable agreement between experimental and theoretical data is observed. Likewise, the standard deviation, σ, reported in columns 6 and 7 shows that the current distribution is closely uniform at both electrodes. Furthermore, columns 10 and 11 in Tables 2 and 3 compare the theoretical and experimental values of applied potential difference, U (V), and leakage current. The experimental leakage currents are always higher than the theoretical ones and the opposite is detected for the applied potential difference. The discrepancies observed, mainly in the leakage current prediction, may be attributed to the gases evolved at the electrodes, which increase the effective resistivity of the electrolyte in the interelectrode gap, raising the leakage current. The gases also produce bubble-induced convection altering the hydrodynamics in the solution phase. Both factors may influence the performance of the reactor and they have not been considered in the mathematical modelling. A similar conclusion

Table 2
Summary of experimental results of current distribution. Anode: nickel. Cathode: nickel.

c_{NaOH}/mol dm^{-3}	R/Ω	I/A	d_r/%		σ/%		Wa_{Bi}		Th.	Exp.
			Terminal	Bipolar	Terminal	Bipolar	$\times10^4$			
1	97.37	0.996	2.33	5.63	3.269	6.895	8.52	U/V	4.76	4.51
								I^*/mA	11.40	21.90
		2.998	2.97	3.49	3.503	4.327	2.83	U/V	6.24	5.97
								I^*/mA	18.85	28.88
		5.007	3.48	2.90	4.965	3.838	1.69	U/V	7.63	7.29
								I^*/mA	25.80	34.64
3	54.35	1.008	3.19	4.45	4.757	5.841	15.08	U/V	4.47	4.16
								I^*/mA	17.78	39.15
		3.006	2.20	3.48	2.813	4.369	5.05	U/V	5.38	5.09
								I^*/mA	25.99	46.41
		4.999	2.68	3.13	3.350	4.194	3.04	U/V	6.20	5.86
								I^*/mA	33.32	53.64

Table 3
Summary of experimental results of current distribution. Anode: nickel. Cathode: stainless steel.

c_{NaOH}/mol dm^{-3}	R/Ω	I/A	d_r/%		σ/%		Wa_{Bi}		Th.	Exp.
			Terminal	Bipolar	Terminal	Bipolar	$\times10^4$			
1	97.37	0.996	4.86	6.08	7.229	7.178	10.17	U/V	5.01	4.71
								I^*/mA	12.83	20.64
		2.988	4.23	4.67	5.654	6.578	3.39	U/V	6.46	6.11
								I^*/mA	20.30	27.06
		4.983	4.09	5.17	5.321	6.666	2.03	U/V	7.92	7.38
								I^*/mA	27.42	34.18
3	54.35	1.010	6.97	8.59	9.755	10.067	17.97	U/V	4.73	4.41
								I^*/mA	20.31	40.99
		2.992	5.42	8.62	7.019	11.146	6.07	U/V	5.67	5.27
								I^*/mA	29.01	49.35
		4.993	3.90	5.41	5.476	6.436	3.64	U/V	6.50	6.01
								I^*/mA	36.61	55.87

was obtained in the previous work [19] with a stationary electrolyte.

Fig. 4 reports an increase in the experimental fraction of the leakage current as the bipolar Wagner number increases because of the decrease in the polarization resistance when the current is augmented. However, the fraction of leakage current is small in all cases, which justifies the uniform current distribution observed for this reactor.

3.2. Mass transfer studies

The local mass-transfer coefficient, k_m (m s^{-1}), was calculated from the limiting current at each segment and the reactant concentration using the following equation

$$k_m(y) = \frac{I_{lim}(y)}{\nu_e FAc} \quad (10)$$

where I_{lim} (A) is the limiting current, A (m^2) is the electrode surface area, c (mol m^{-3}) is the concentration of the electroactive species, ν_e is the number of electrons interchanged and F (96,485 C mol^{-1}) is the Faraday constant.

Fig. 5 shows the ratio between the local mass-transfer coefficient and its mean value as a function of the axial position in the reactor. The points for the empty reactor, (●) represent the

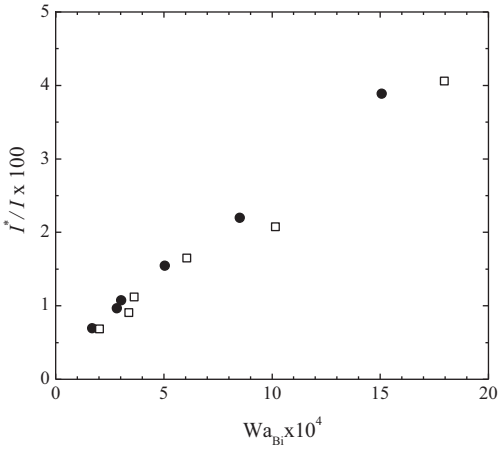

Fig. 4. Fraction of leakage current as a function of the bipolar Wagner number. (●) Ni cathode; (□) stainless steel cathode.

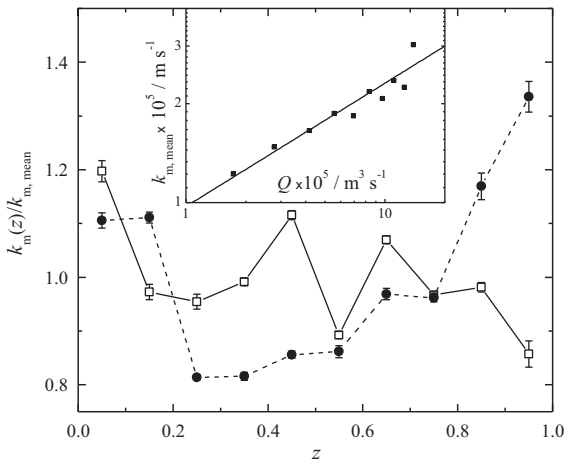

Fig. 5. Ratio between the local mass-transfer coefficient to the mean value as a function of the axial position in the reactor. (●) Empty reactor; (□) plastic beads 3 mm diameter as turbulence promoter. Vertical segments: standard error. Inset: mean values of the mass-transfer coefficient as a function of the volumetric flow rate.

mean value of six experiments at different volumetric flow rates, Q ranging from 3.33×10^{-5} to 20×10^{-5} m^3 s^{-1} and show a pronounced variation with the position. However, when the reactor is filled with plastic beads, (□) the local mass-transfer coefficient becomes more uniform along the reactor. Each point is the mean value of twelve experiments at different volumetric flow rates lying from 1.67×10^{-5} to 16.17×10^{-5} m^3 s^{-1}. Due to the entrance effects only the first segment shows a mass-transfer coefficient 20% higher than the mean value, whereas in the other segments the variation is between ±10%, which represents an acceptable result for mass-transfer studies. The inset in Fig. 5 reports, in a double logarithmic plot, typical mean values of the mass-transfer coefficient as a function of the volumetric flow rate. Likewise, the correlation of the experimental results yields an exponent for the volumetric flow rate of 0.4. A similar value was reported in [11] for a rectangular channel with the SU promoter, which is a specially designed plastic grid with triangular threads of polypropylene and is supplied with flow distributors at the inlet and the outlet.

3.3. Residence time distribution

3.3.1. Theoretical considerations

The temporal behaviour of an electrochemical reactor without reaction according to the dispersion model is given by

$$\frac{\partial c(T,\ z)}{\partial T} = \frac{1}{\mathrm{Pe}} \frac{\partial^2 c(T,z)}{\partial z^2} - \frac{\partial c(T,\ z)}{\partial z} \tag{11}$$

being Pe the Peclet number, T the dimensionless time and z the normalized axial coordinate, which are defined as:

$$\mathrm{Pe} = \frac{uL}{\varepsilon D_L}, \quad T = \frac{t}{\tau}, \quad \text{and} \quad z = \frac{y}{L} \tag{12}$$

where u (m s^{-1}) is the superficial liquid flow velocity, D_L (m^2 s^{-1}) is the dispersion coefficient, ε is the porosity, t is the time (s) and τ(s) is the reactor residence time. Solving Eq. (11) for an open system with the following initial and boundary conditions

$$T = 0 \quad c(0,\ z) = 0 \tag{13}$$

$$z = 0 \quad c(T,\ 0) = a\delta(T - 0) \tag{14}$$

here a (mol m^{-3}) is a parameter and δ is the Dirac delta function,

$$z \to \infty \quad c(T, \infty) = 0 \tag{15}$$

it results for the normalized outlet concentration

$$E = \sqrt{\frac{\mathrm{Pe}}{4\pi T^3}}\, \mathrm{e}^{-\left[\frac{\mathrm{Pe}(1-T)^2}{4T}\right]} \tag{16}$$

Eq. (16) was given by Gibilaro [20] and in [21] it was demonstrated that for Pe numbers higher than 5 can be used to correlate experimental results.

3.3.2. Residence time distribution results

Fig. 6 shows typical residence time distributions for the empty plate with the inclined segmented electrodes or with two different turbulence promoters. Similarly, Fig. 7 reports typical residence time distributions for the empty frame or with turbulence promoters. The residence time distributions for the reactor with two plates and one frame are shown in Fig. 8 for different volumetric flow rates. In these figures a dimensionless time referred to the mean residence time, t_mean (s), was used, which was calculated as

$$t_\mathrm{mean} = \frac{\int_0^\infty tc(t)\ dt}{\int_0^\infty c(t)\, dt} \tag{17}$$

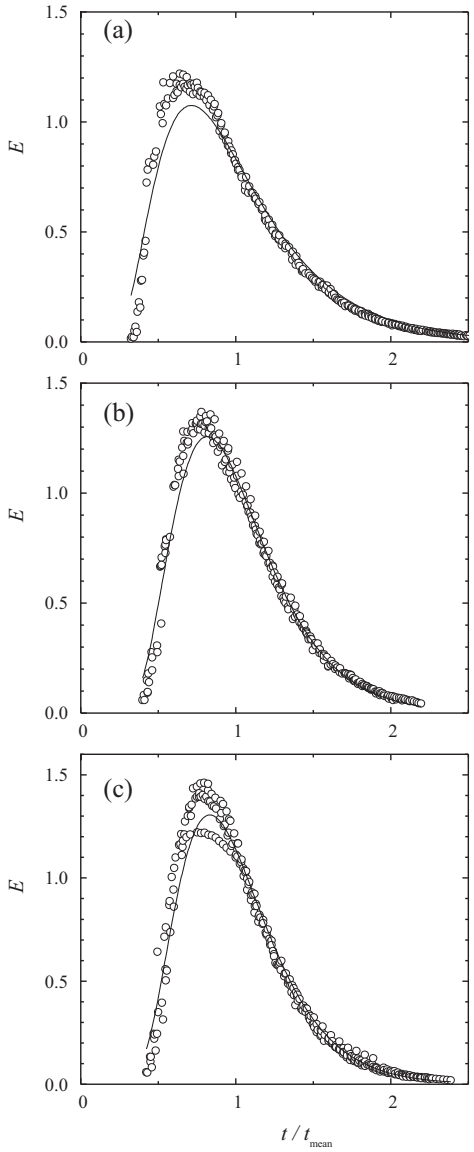

Fig. 6. Residence time distribution for the plate with inclined electrodes. (a) Empty plate; (b) plastic beads as turbulence promoters, 3 mm diameter; (c) glass beads as turbulence promoter, 4 mm diameter. Continuous lines: correlation according to Eq. (16). $Q = 2.27 \times 10^{-5}$ m^3 s^{-1}.

Table 4
Summary of experimental Peclet numbers for the plate with electrodes and for the frame.

	$Q \times 10^6$/m^3 s^{-1}	Empty		Glass beads 4 mm		Plastic beads 3 mm	
		Pe	τ/s	Pe	τ/s	Pe	τ/s
Plate with electrodes	5.19	8.9 ± 0.4	23.59	11.4 ± 0.3	18.82	13.3 ± 0.2	14.11
	13.14	10.3 ± 0.4	9.49	15.7 ± 0.4	7.65	16.9 ± 0.2	5.48
	22.70	8.7 ± 0.2	5.56	16.3 ± 0.4	4.41	14.6 ± 0.3	3.18
Frame	5.19	3.1 ± 0.1	25.10	7.5 ± 0.3	14.06	7.1 ± 0.3	12.79
	13.14	2.2 ± 0.2	9.86	11.4 ± 0.2	5.44	13.0 ± 0.2	5.00
	22.70	1.69 ± 0.03	5.75	11.5 ± 0.3	3.19	12.6 ± 0.4	2.97

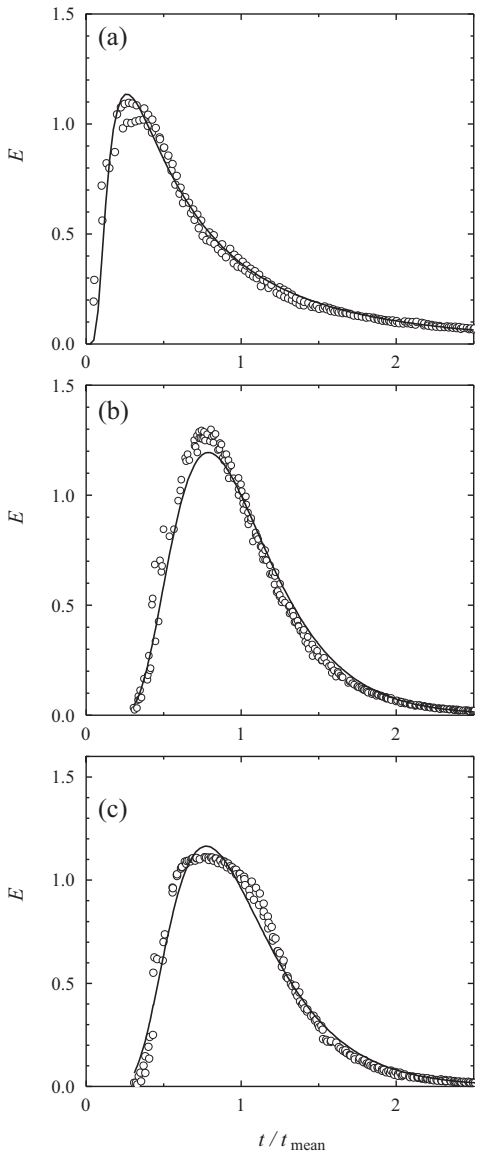

Fig. 7. Residence time distribution for the frame. (a) Empty frame; (b) plastic beads as turbulence promoters, 3 mm diameter; (c) glass beads as turbulence promoter, 4 mm diameter. Continuous lines: correlation according to Eq. (16). $Q = 2.27 \times 10^{-5}$ m^3 s^{-1}.

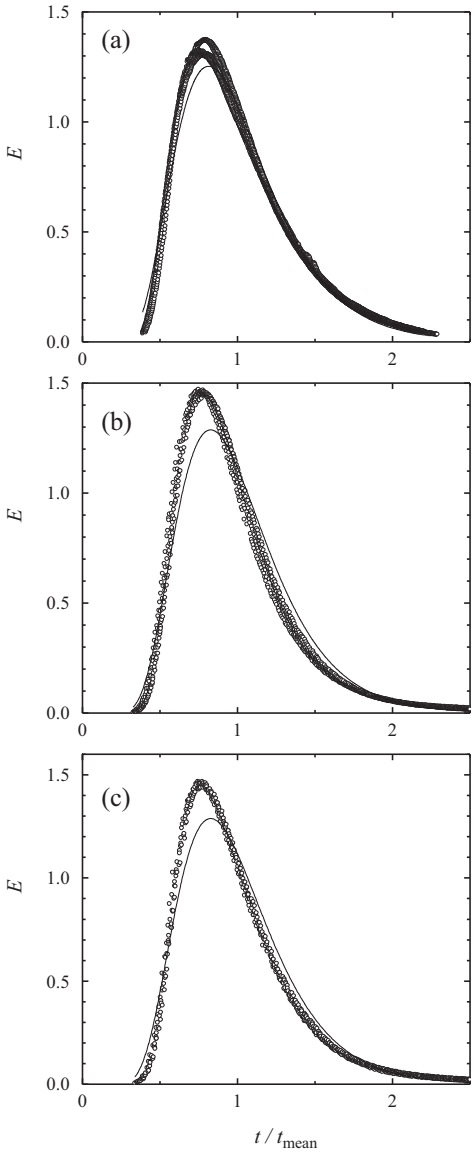

Fig. 8. Residence time distribution for the reactor, monopolar arrangement, with plastic beads as turbulence promoters, 3 mm diameter. (a) $Q = 4.31 \times 10^{-6}$ m^3 s^{-1}; (b) $Q = 1.11 \times 10^{-5}$ m^3 s^{-1}; (c) $Q = 1.88 \times 10^{-5}$ m^3 s^{-1}. Continuous lines: correlation according to Eq. (16).

The experimental points correspond to five independent experiments and the full line represents their correlation by means of a weighted least square method applied to Eq. (16). Tables 4 and 5 summarize the Peclet number. It can be observed that with the use of turbulence promoters the reactor, the plate with inclined electrodes as well as the frame can be properly modelled by the dispersion model with a Peclet number near to 10. For this value of the Peclet number the behaviour of the reactor is close to that given by the plug flow model.

Table 5
Summary of experimental Peclet numbers for the reactor. Plastic beads 3 mm.

$Q \times 10^6$/m^3 s^{-1}	Pe	τ/s
4.31	14.4 ± 0.2	44.89
7.61	16.0 ± 0.2	25.40
11.06	15.6 ± 0.2	17.48
14.70	15.2 ± 0.3	13.15
18.76	15.7 ± 0.3	10.30
22.87	16.7 ± 0.4	8.45

4. Conclusions

- The theoretical and experimental results show that this reactor with a bipolar connection presents a small leakage current, lower than 4%, and thus the secondary current distribution is even.
- When the reactor is filled with a turbulence promoter, the mass transfer conditions are closely uniform along the electrode. A variation of ±10% from the mean value was observed.
- The fluidodynamic behaviour of the reactor can be properly represented by the dispersion model with a Peclet number near to 10 or can be approached by the plug flow model.
- Taking into account the above conclusions, this reactor represents a suitable device for laboratory trials and process development.

Acknowledgements

This work was supported by the Agencia Nacional de Promoción Científica y Tecnológica (ANPCyT), Consejo Nacional de Investigaciones Científicas y Técnicas (CONICET) and Universidad Nacional del Litoral (UNL) of Argentina.

References

[1] F.C. Walsh, A First Course in Electrochemical Engineering, Alresford Press, Alresford, 1993 (Chapter 8, p. 273).
[2] J.K. Hammond, D. Robinson, C.J. Brown, D. Pletcher, F.C. Walsh, Dechema-Monographs 123 (1991) 299.
[3] C.J. Brown, D. Pletcher, F.C. Walsh, J.K. Hammond, D. Robinson, J. Appl. Electrochem. 22 (1992) 613.
[4] C.J. Brown, D. Pletcher, F.C. Walsh, J.K. Hammond, D. Robinson, J. Appl. Electrochem. 23 (1993) 38.
[5] C.J. Brown, D. Pletcher, F.C. Walsh, J.K. Hammond, D. Robinson, J. Appl. Electrochem. 24 (1994) 95.
[6] P. Trinidad, F.C. Walsh, Electrochim. Acta 41 (1996) 493.
[7] C. Bengoa, A. Montillet, P. Legentilhomme, J. Legrand, Ind. Eng. Chem. Res. 39 (2000) 2199.
[8] P. Trinidad, C. Ponce de León, F.C. Walsh, Electrochim. Acta 52 (2006) 604.
[9] F.A. Rivera, M.R. Cruz-Díaz, E.P. Rivero, I. González, Electrochim. Acta 56 (2010) 361.
[10] M. Chikhi, M. Rakib, Ph. Viers, S. Laborie, A. Hita, G. Durand, Desalination 149 (2002) 375.
[11] L. Carlsson, B. Sandegren, D. Simonsson, M. Rihovsky, J. Electrochem. Soc. 130 (1983) 342.
[12] A. Montillet, J. Comiti, J. Legrand, J. Appl. Electrochem. 23 (1993) 1045.
[13] C. Bengoa, A. Montillet, P. Legentilhomme, J. Legrand, J. Appl. Electrochem. 27 (1997) 1313.
[14] J. González-García, J.A. Conesa, J. Iniesta, V. García-García, V. Montiel, A. Aldaz, ICHEME Symp. Ser. 145 (1999) 51.
[15] J. González-García, A. Frías, E. Expósito, V. Montiel, A. Aldaz, Ind. Eng. Chem. Res. 39 (2000) 1132.
[16] D. Bergner, K. Hannesen, in: K. Wall (Ed.), Modern Chlor-alkali Technology, vol. 3, Ellis Horwood Ltd., Chichester, 1986 (Chapter 13, p. 162).
[17] M. Shirkhanzadeh, M. Ajersch, L.W. Shemilt, J. Appl. Electrochem. 23 (1993) 463.
[18] G. Kreysa, H.-J. Külps, J. Electrochem. Soc. 128 (1981) 979.
[19] E.R. Henquín, J.M. Bisang, J. Appl. Electrochem. 38 (2008) 1259.
[20] L.G. Gibilaro, Chem. Eng. Sci. 33 (1978) 487.
[21] A.N. Colli, J.M. Bisang, Electrochim. Acta, under review, EAST11-0297R.